processes

MDPI

Article

Preparation and Composition Analysis of Modified Asphalt for Preparing Carbon Fiber from Coal Direct Liquefaction Asphalt

Yong Liu [1], Chenguang Jiang [2,*] and Miao Gao [1]

[1] Ordos Coal to Liquid Branch of China Shenhua Coal to Liquid and Chemical Co., Ltd., Ordos 017209, China
[2] National Institute of Clean and Low Carbon Energy, Beijing 102211, China
* Correspondence: jiangcg521@126.com; Tel./Fax: +86-010-57337583

Abstract: The modified asphalt with high softening point was prepared by air oxidation polymerization with coal liquefied asphalt as raw material. The quality control model regarding the coking value and softening point of the product were established based on the DFSS (Design for Six Sigma) and RSM (response surface method). By means of elemental analysis, infrared, XPS, XRD, nuclear magnetic, MALDI-TOF and other characterization methods, the composition and structure characteristics of the modified asphalt were analyzed. Using the target product as raw material, general base asphalt carbon fiber was prepared by spinning, pre-oxidation and carbonization. The results show that the fitting effect of the quality control model about the coking value and softening point of the product is good, and the operating window range of the polymerization process parameters corresponding to the preparation of target product is wide. It can be found that the oxidation time and oxidation temperature has the most significant effect on the coking value and softening point of products, respectively, and all of them show a positive correlation. The dealkylation reaction and oxidative crosslinking reaction were carried out at the same time, and the bridging products of methylene bridging products, ether–oxygen bonds, carbonyl bonds, anhydride bonds and other oxygen-containing groups were generated. The properties of carbon fiber prepared with the target product are better: the tensile strength is 775 MPa, the elastic modulus is 68.6 GPa and the elongation at break is 1.13%.

Keywords: softening point; coking value; response surface; oxidation polymerization; operation window

check for updates

Academic Editor: Vincenzo Russo

Received: 5 May 2025
Revised: 28 May 2025
Accepted: 9 June 2025
Published: 13 June 2025

Citation: Liu, Y.; Jiang, C.; Gao, M. Preparation and Composition Analysis of Modified Asphalt for Preparing Carbon Fiber from Coal Direct Liquefaction Asphalt. *Processes* **2025**, *13*, 1869. https://doi.org/10.3390/pr13061869

Copyright: © 2025 by the authors. Licensee MDPI, Basel, Switzerland. This article is an open access article distributed under the terms and conditions of the Creative Commons Attribution (CC BY) license (https://creativecommons.org/licenses/by/4.0/).

1. Introduction

Coal liquefaction asphalt is a heavy by-product produced by full hydrogenation (500 °C, 19 MPa hydrogen pressure) in the process of direct coal liquefaction. The liquefaction asphalt has a higher carbon residue rate compared with petroleum asphalt and a higher hydrogen content compared with coal tar asphalt, resulting in the prepared product having a high yield and certain fluidity, which is suitable for the preparation of carbon fiber. In addition to having high carbon content similar to coal tar asphalt, it also has structural characteristics such as lower sulfur content, lower quinoline insoluble content, higher softening point, suitable thick ring condensation degree and adjustable component distribution. Therefore, it is a unique raw material for preparing high-performance carbon materials [1]. Coal tar asphalt and coal liquefaction asphalt have a wide molecular weight distribution and complex structure. Researchers often establish the average structure model of asphalt by means of extraction separation, infrared and nuclear magnetic means [2,3]. It has been found that there are a number of alkyl side chains or cycloalkanes with different lengths

around the aromatic ring of coal liquefaction asphalt, which may lead to oxidation, polymerization and crosslinking reactions more easily than coal tar asphalt [4–6]. At present, most of the asphalt-based carbon materials reported in the literature come from coal tar asphalt, petroleum asphalt and biomass asphalt [7,8]. However, there are few reports on the preparation of carbon materials based on liquefaction asphalt.

In order to improve the carbon yield of coal tar asphalt and achieve its high-value utilization, extensive and in-depth research has been carried out at home and abroad on the modification of coal tar asphalt. Common modification methods include distillation, blending, heat treatment, air oxidation, hydrogenation, alkylation, co-carbonization, etc. [9–14]. Among them, air oxidation and nitrogen thermal condensation are one of the most widely used methods. The reaction of dehydrogenation condensation, aromatization and crosslinking in air oxidation produces larger molecules, which has higher product yield and is easy to be scaled up for industrialization. Modified asphalt obtained by air oxidation generally refers to asphalt materials with softening point greater than 240 °C and coking value greater than 80%, which is the precursor of a variety of high-quality carbon materials. Asphalt with high softening point can be used as coated asphalt in lithium anode materials to modify holes, grooves, cracks and other defects in graphite and improve the electrochemical reversible capacity and cycle performance of the material [15]. In addition, high softening point asphalt can also be used as spinnable asphalt, through melt spinning, pre-oxidation, carbonization to produce general grade carbon fiber, high-temperature smelting insulation felt, conductive filler and other fields [16]. Guo [17] reported the oxidation reaction mechanism of ethylene tar during the oxidation reaction. The side chains of the aromatic compounds firstly react with oxygen to form aldehydes and alcohols, at the same time forming peroxy radicals, then the aromatic compounds with peroxy radicals undergo polymerization or condensation reactions to form larger molecules. Fernández [18] reported that the air oxidation method increases the softening point of coal tar asphalt, which increases the carbon residue rate of asphalt base products without affecting the fluidity of impregnating agent asphalt. The main process of oxidation is dehydrogenation polymerization, and crossing-linking of oligomers occurs. Zhou [19] reported that the carbon microfibers were synthesized from coal liquefaction residue by arc-jetplasma method, which is a preliminary exploration, and the reaction mechanism is not fully revealed. Meanwhile, this work provides a new idea for the preparation of carbon materials from coal liquefaction asphalt. However, there are few reports on the preparation of modified asphalt with high softening point by oxidation polymerization of coal liquefaction asphalt. The high-value utilization of coal liquefaction asphalt is conducive to extending the product chain of coal direct liquefaction technology, improving the economy of the coal-to-oil industry chain, which is of great significance to ensuring the large-scale development of the coal-to-oil industry.

In order to fully utilize the high carbon and low sulfur characteristics of coal liquefaction asphalt, the preparation of the precursor of high-end carbon materials such as coated asphalt and spinnable asphalt (coking value > 80%, softening point > 240 °C) are treated as the target product in this work. The experimental research on the oxidation polymerization experiment of coal liquefaction asphalt to prepare high softening point asphalt were carried out based on the DFSS (Design for Six Sigma) and RSM (response surface method), and the range of oxidation process parameters was determined. Meanwhile, the spinnability application performance evaluation of the optimized products was carried out and compared with the mechanical performance of commercial carbon fibers from the preparation of coal tar asphalt, which provides a new path for the high-value utilization of coal liquefaction asphalt and the preparation of high-end carbon materials.

2. Experimental Section

2.1. Raw Material

The raw material used in the experiment is coal liquefaction asphalt from coal-to-oil production in China Shenhua Coal to Liquid Chemical Co., Ltd., Inner Mongolia, China. The reagents n-heptane, quinoline and toluene used to test the composition of the raw material asphalt group are all from Enokine reagents and are all analytically pure.

2.2. Experimental Method

The modified asphalts with high softening point were prepared by oxidation polymerization of coal liquefaction asphalts. The oxidation polymerization equipment used in the experiment is the PARR 4577 high-pressure reactor (Parr Instrument company, Moline, IL, USA). The reaction temperature was 290 °C~340 °C, the reaction atmosphere was air, the air flow rate was 1~4 L/min, the reaction time was 1~4 h and the stirring rate was 400 rpm. It needs to be particularly emphasized that all the oxidative polymerization reactions in this work were carried out under normal pressure.

2.3. Carbon Fiber Preparation

Further, the modified asphalt product with a coking value greater than 80% and a softening point higher than 240 °C is called the target product, which is used as the raw material for preparing carbon fiber. The general grade carbon fiber is prepared by a spinning, pre-oxidation and carbonization process from the target product. Firstly, fiber filaments were prepared using the M12 melt spinning machine. Secondly, pre-oxidized fiber was obtained by weighing the original filament at about 2 g and putting it into the pre-oxidized furnace. The oxidation temperature was set at 340 °C under an air atmosphere, and the pre-oxidized fiber was obtained for a certain period of time. Then, the obtained pre-oxidized fiber was placed in a tube furnace and carbonized under nitrogen atmosphere at 1300 °C, and finally, the liquefaction asphalt base general grade carbon fiber was obtained.

2.4. Material Characterizations

The softening points of raw asphalt used in the experiment and modified asphalt with high softening point were determined by global method according to GB/T2294-2019 [20] and ISO 5940-2: 2007 [21]. The content of quinoline insoluble matter was determined according to GB/T 2293-2019 [22]. The elemental analysis was determined by EA3000 type element analyzer produced by Leeman Company of Germany (Hamburg, Germany). The reference standards for the analysis methods of hydrocarbon, nitrogen, sulfur and oxygen are SH/T 0656-2017 [23], SH/T 0704-2010 [24], GB/T 17040-2008 [25] and SH/T 0986-2019 [26], respectively.

Asphaltic raw materials and oxidized polymerized solid products with high softening point asphalt were characterized by VERTEX 70 Fourier transform infrared spectrometer (Bruker Corporation, Billerica, MA, USA), and the organic functional group composition of the sample was determined. The resolution was as high as 0.16 cm^{-1}, the measurement spectral range was 4000–400 cm^{-1} and the scanning times were 36 times/s.

XPS tests of C1s, O1s, S2p and N1s were performed on asphalt raw materials and modified asphalt with high softening point prepared by X-ray photoelectron spectrometer (AXIS Ultra DLD, made in Kratos Analytical Ltd., Manchester, UK) to analyze the existence forms of oxygen, nitrogen and sulfur in raw materials and products. The obtained maps were fitted by peaks using OriginPro 2021b software.

The D8 ADVANCE XRD analyzer with Cu target and Kα radiation source produced by Bruker, Karlsruhe, Germany, was used to analyze the crystal composition, lattice structure and other information of asphalt raw materials and oxidation polymerization products. Among them, the working voltage is 40 kV, the working current is 40 mA, the scanning

range is 5~80°, the scanning rate is 5°/min and the step size is 0.013°. The grain size Lc and La of the samples were calculated by Equations (1) and (2) [27,28].

$$L_c = \frac{K\lambda}{\beta_c \cos\theta_c} \quad (1)$$

$$L_a = \frac{1.84\lambda}{\beta_a \cos\theta_a} \quad (2)$$

where K = 0.89, and wavelength λ = 0.15406 nm. β_c and β_α represent the maximum half-peak width (FWHM) of peak 002 and peak 100, respectively. θ_c and θ_α are the diffraction angles of C (002) and C (100), respectively. The area of the two carbon peaks can be calculated by fitting (002) peaks by peaks, so as to obtain the content Ig of orderly carbon microcrystals in carbon-rich materials. Ig is calculated by Equation (3) [29]:

$$Ig = I_{26}/(I_{22} + I_{26}) \quad (3)$$

Among them, I_{22} represents the area of the carbon peak of the amorphous carbon structure, and I_{26} represents the peak area of the carbon microcrystals, the arrangement of which tends to be regular.

13C-NMR testing of the products and asphalt raw materials were performed on the Bruker Avance Neo 400WB nuclear magnetic resonance spectrometer in Bruker Corporation, Rheinstetten, Germany, and the aromainess of the samples were calculated based on the solid nuclear magnetic carbon spectrum by Equation (4) [30,31]:

$$f_A = A_a/(A_a + A_s) \quad (4)$$

where A_a represents the integral area of aromatic carbon, and A_s represents the integral area of saturated carbon.

The molecular weight of raw materials and products was tested on the Bruker ultra-flextreme MALDI-TOF/TOF (Bruker Corporation, Bremen, Germany) matrix assisted laser desorption time-of-flight mass spectrometer using TCNQ as the substrate.

2.5. Experimental Design

Oxidation time, oxidation temperature and air flow were selected as factors, and coking value and softening point were selected as response values. Through customized experiment design, JMP 14.0 software was used to carry out regression analysis of experimental results, and the transfer function between the required factors and the response values was established. As shown in Table 1, 5 levels were set for each factor, including high and low axial points and center points. The central point experiment was repeated twice to check the reproducibility of the experiment, controlling the rationality of model fitting and evaluating the pure error of the experiment. All experiments were conducted in random order. Experimental numbers were randomly composed to reduce systematic errors [32].

Table 1. Experimental factors and level settings.

Factors	Code	Codin and Level					Unite
		−1	−	0	+	+1	
Oxidation time	X_1	1	1.54	2.5		4	h
Oxidation temperature	X_2	290		315		340	°C
Air flow rate	X_3	0.5		1.25	1.483	2	L/min

3. Results and Discussion

The raw material used in this work is coal liquefaction asphalt. The macro-property analysis of the raw material and the results of elemental analysis are shown in Tables 2 and 3, respectively, which provide reference for the analysis of the composition of subsequent products and reaction mechanism, where HS, HI-TS, TI-QS and QI represent the contents of n-heptane soluble matter; n-heptane insoluble and toluene soluble matter; toluene insoluble and quinoline soluble matter; and quinoline insoluble matter, respectively.

Table 2. Analysis of basic properties of coal liquefaction asphalt raw materials.

Sample	Softening Point/°C	Coking Value/%	Ash Content/%	HS/%	HI-TS/%	TI-QS/%	QI/%
coal liquefaction asphalt	150	67	0.110	29.62	44.4	24.49	0.110

Table 3. Elemental analysis of coal liquefaction asphalt raw materials.

Sample	C/%	H/%	N/%	S/%	O/%
coal liquefaction asphalt	90.30	5.32	1.10	0.08	2.184

It can be found that the ash content of coal liquefaction asphalt is about 1000 ppm, and the entire experimental design does not consider the influence of changes in the ash content of raw materials on the properties of the products. The oxygen content of raw material is 2.184%, with lower sulfur content, which can be used to determine the degree of change in oxygen content of the product after the oxidative polymerization reaction.

3.1. Establishing the Regression Model

Based on the principle of customized experimental design, the experimental combination design of two central points with three factors and five levels was carried out according to Table 1, and the influence of each factor on the oxidation process of asphalt was investigated. The influence on the properties of asphalt with high softening point of the product was analyzed.

The experimental results are shown in Table 4, and the response surface method is used to analyze the experimental results. Response value coking value and softening point are denoted as $Y_{coking\ value}$ and $Y_{softening\ point}$, respectively. Oxidation temperature, oxidation time and air flow rate of the factors under investigation are denoted as X_1, X_2 and X_3, respectively. Then, the fitting model between the factors under investigation and the response value can be simplified into Equations (5) and (6):

$$Y_{coking\ value} = 31.475 + 1.733 \times X_1 + 0.121 \times X_2 + 3.704 \times X_3 + 0.033(X_1 - 2.545) \times (X_2 - 315) \quad (5)$$

$$Y_{softening\ point} = -267.160 + 15.575 \times X_1 + 1.408 \times X_2 + 46.8136 \times X_3 + 0.877\ (X_2 - 315) \times (X_3 - 1.206) - 31.342\ (X_3 - 1.207) \times (X_3 - 1.207) \quad (6)$$

3.2. Model Variance Analysis

The adequacy and significance of the model were tested by variance analysis of the regression models of "coking value" and "softening point". The variance analysis of each parameter was carried out by correlation coefficient R^2, correction correlation coefficient R^2_{Adj}, *p*-value, residual normality test, F-value and other indexes [32,33]. Among them, the *p*-value is considered to be less than 0.05 in statistics, which means that this parameter item is considered significant and can reflect the fraction of residual in the regression equation

in the total variance. When the R^2 is higher, the model's significance can be accepted by the design, and the model does not have the problem of "underfitting". If the R^2 is close to R^2_{Adj}, it can be considered that the model has high fitting degree and rationality [32]. The residual represents the difference between the predicted value and the measured value. The goodness of fit test value W of the residual distribution is bigger than 0.05, indicating that the residual follows a normal distribution and the model is real and reliable. The model test statistic value of F represents the ratio of the variance and residual of the regression model. The value of F is larger and the residual is smaller, indicating the more significant influence of the corresponding parameter item on the model [34].

Table 4. DOE design matrix and experimental results.

	X_1/h	X_2/°C	X_3/L·min^{-1}	Coking Value/%	QI/%	Softening Point/°C
1	4	315	1.25	82.30	1.89	298.35
2	2.5	315	1.25	80.25	1.45	260.95
3	2.5	290	0.5	73.15	0.20	211.05
4	2.5	340	0.5	77.76	0.83	240
5	1	340	1.483	78.53	0.05	314.2
6	1.54	315	2	79.62	0.99	265.15
7	1	315	0.5	72.93	0.48	203.5
8	4	340	2	87.80	29.87	361.6
9	2.5	315	1.25	79.16	1.61	283.25
10	4	290	2	78.60	0.38	270.35
11	4	315	0.5	77.74	0.41	240.6
12	1	290	1.25	73.57	0.38	204.6

3.2.1. Variance Analysis of the Coking Value

It can be seen from Table 5 that the *p*-value of the regression model about product coking value is smaller than 0.0001, which is significantly less than 0.05, indicating that the model is significant. The regression model established is suitable for the analysis of the coking value of asphalt products. The *p*-value of the model missing fitting item is 0.4888, which is bigger than 0.05, indicating that the missing fitting item caused by pure error is not significant, and the model has higher prediction accuracy [35]. According to the *p*-value of each parameter and the corresponding statistic F value, the significance of the influence of each factor on the coking value of the product is judged. It can be found that oxidation temperature, oxidation time and air flow rate have significant effects on coking value, which follows oxidation temperature > air flow > oxidation time. Meanwhile, the second-order interaction of oxidation time and oxidation temperature also affects the coking value of the product. The correlation coefficient R^2 of the fitted model and the correction determination coefficient R^2_{Adj} are close to 1, and the difference between them is small, indicating that the model has high quality and fitting degree. The goodness of fit test value of the residual W is greater than 0.05, indicating that the residual follows a normal distribution, and the regression model about "coking value" is real and reliable [36].

3.2.2. Variance Analysis of the Softening Point

It can be seen from Table 6 that the *p*-value of the softening point model of asphalt products is smaller than 0.0001, which is significantly less than 0.05, indicating that the model is significant, and the regression model established is suitable for product softening point analysis. The *p*-value of the model missing item is 0.7936, which is bigger than 0.05, indicating that the regression model has a high degree of fitting, and the missing item is not significant relative to the absolute error. The *p*-values of the first-order parameters and second-order interaction terms of the model can be used to judge the significance of the influence of the main effect and interaction effect on the softening point of the products. In

addition, the significance degree of the influence can be judged by the F value of the statistic. Therefore, it can be found that the influence of first-order parameters on the softening point is more significant than that of the second-order interaction. The second-order interaction of oxidation temperature and air flow rate has significant effect on the softening point. The correlation coefficient R^2 of the model and the correction determination coefficient R^2_{Adj} are very close to 1, indicating that the regression model has good prediction accuracy and rationality. The goodness of fit test value of the residual W is greater than 0.05, indicating that the residual follows a normal distribution, and the regression model about "softening point" is real and reliable.

Table 5. Analysis of variance of coking regression model.

Source of Variance	Sum of Squares	Degree of Freedom	Mean Square	F	*p*
Model	182.8351	4	45.7088	40.4666	<0.0001
X_1	52.1271	1	48.9103	43.3010	0.00022
X_2	55.4209	1	54.6436	48.3767	0.00024
X_3	53.3215	1	52.9456	46.8735	0.00031
$X_1 \times X_2$	6.1122	1	6.4827	5.7362	0.04777
Residual	7.9068	7	1.1295	— —	— —
Misfitting term	7.3127	6	1.2187	2.0517	0.4888
Pure error	0.59405	1	0.59405	— —	— —
$R^2 = 0.958$	182.8351				
$R^2_{Adj} = 0.935$	52.1271				
$W = 0.535 > 0.05$	55.4209				

Table 6. Analysis of variance of softening point model.

Source of Variance	Sum of Squares	Degree of Freedom	Mean Square	F	*p*
Model	23,985.089	5	4797.02	33.4063	<0.0001
X_1	3685.0149	1	3685.0149	25.6624	0.00025
X_2	7286.2815	1	7286.2815	50.7415	0.00039
X_3	8477.6723	1	8477.6723	59.0383	0.00230
$X_2 \times X_3$	1095.7642	1	1095.7642	7.6309	0.03275
Residual	861.5763	6	143.5961	——	——
Misfitting term	606.1963	5	121.239	0.4747	0.7936
Pure error	255.3800	1	255.3800	——	——
$R^2 = 0.965$					
$R^2_{Adj} = 0.936$					
$W = 0.717 > 0.05$					

3.3. Response Surface Analysis of the Regression Model

Through the variance analysis of the regression model, it can be seen that the influence of each factor on the coking value and softening point is not a simple linear relationship but a curved surface relationship. Meanwhile, the influence of each factor and the interaction between the factors on the response value were analyzed, and the oxidation mechanism was further analyzed by the factor interaction diagram, surface diagram and Pareto chart. The Pareto diagram can describe independent variables and the normalization effect between them, and the larger the normalization effect, the more significant the influence of the parameter term. The factor interaction diagram describes how the response value changes with the variation of one factor when another factor is at a low or high level. It should be noted that the dotted lines are parallel to each other, indicating that there is no interaction between the two factors. On the contrary, solid lines indicate that there is an interaction between the two factors, which means that the influence of one independent variable on the response value will vary depending on the set value of the other independent variable. For

the response surface diagram, the two independent variables form a plane in the diagram, and the response value serves as the coordinate axis perpendicular to this plane. Each point on the surface represents the predicted value of the response variable under a specific combination of independent variable values. Therefore, the surface diagram describes how the other two factors affect the change of response value when one of the factors is at the central level.

3.3.1. Response Surface Analysis of the Coking Value

As can be seen from Figure 1, oxidation time has the most significant influence on the coking value of asphalt products with high softening point, followed by oxidation temperature and air flow, and all of them show a positive correlation. In addition, the proportion of oxidation time, oxidation temperature and air flow is 84%, and the proportion of the second-order interaction is 16%. In short, a curved relationship is presented between the examined factors and the response values of the coking value.

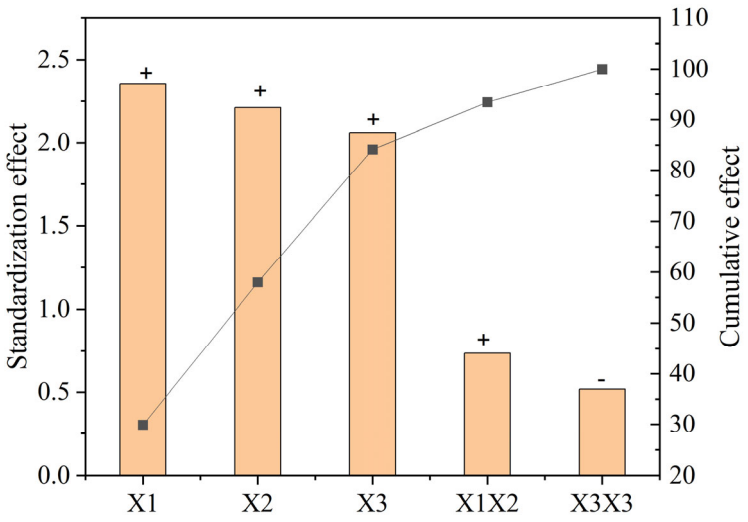


Figure 1. Influence of each factor and its standardization effect on $Y_{coking\ value}$.

As shown in Figure 2, there is an interaction between oxidation temperature and oxidation time, and the analysis results are consistent with the analysis of variance. When the oxidation temperature is 290 °C or 340 °C, the coking value of the product increases with the increase in oxidation time. When the oxidation temperature is at a high level, the increase in the coking value of the product is relatively large with the increase in oxidation time. When the oxidation time is 1 h or 4 h, the coking value of the product increases with the increase in oxidation temperature. Similarly, compared with the shorter oxidation time, the coking value of the product increases greatly with the increase in oxidation temperature when the oxidation time is 4 h. It can be inferred that the reaction rate of the whole reaction system is accelerated when the reaction temperature is higher, and the light components escape faster. The longer oxidation time can make the oxidation crosslinking reaction more complete, and the big asphalt aromatic molecules form with higher molecular weight, resulting in the coking value of the products increasing [37]. Therefore, the influence degrees of oxidation temperature and oxidation time on the coking value may vary depending on the set values of them. As shown in Figure 3, the displayed curved surface is not a very regular plane, with slight distortion, indicating there is an interaction between the oxidation temperature and the oxidation time, which is consistent with the result in Figure 2.

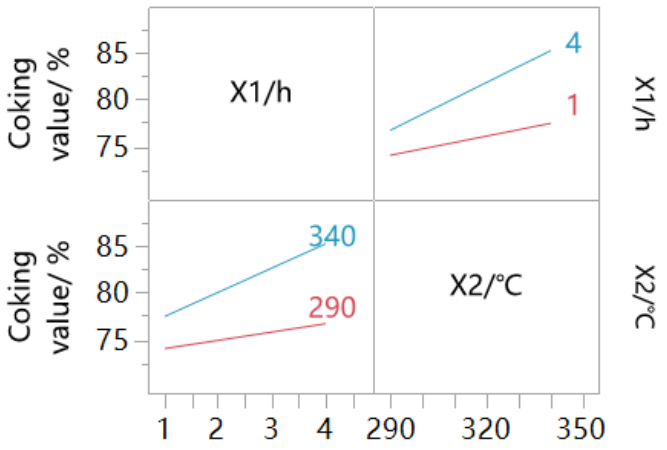


Figure 2. The factor interaction diagram of $Y_{coking\ value}$.

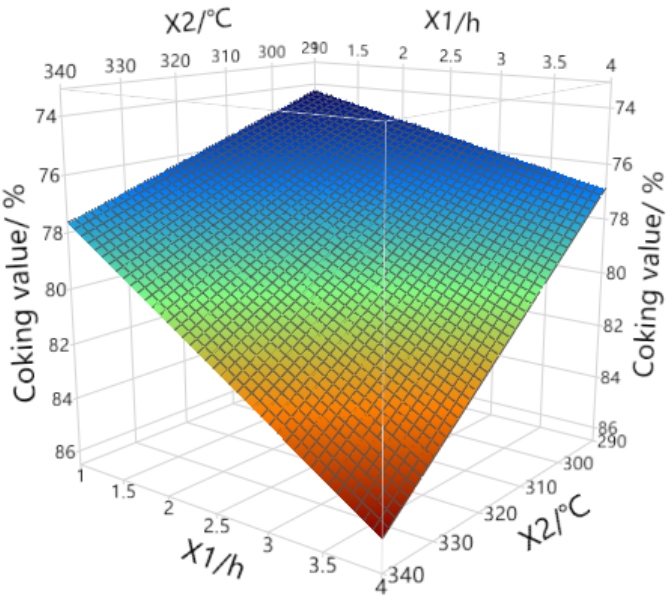


Figure 3. Response surface diagram of $Y_{coking\ value} = f(X_1,\ X_2)$.

3.3.2. Response Surface Analysis of the Softening Point

As can be seen from Figure 4, oxidation temperature has the most significant influence on the softening point of the product, followed by the air flow, the oxidation time, the interaction of oxidation temperature and air flow and the second-order interaction of air flow. Among them, the proportion of the primary parameter is 80%, and the proportion of the second-order interaction is 20%. In short, a curved relationship is presented between the examined factors and the response values of the softening point.

As can be seen from Figure 5, when the air flow rate is 1 L/min or 4 L/min, the softening point of the product shows an increasing trend with the increase in oxidation temperature. Meanwhile, the softening point has an obvious increasing trend under the condition that the air flow rate is larger, which may be due to that the oxygen concentration of the whole reaction system is sufficient, which aggravates the free radical polymerization reaction. When the oxidation temperature is 290 °C, the softening point of the product shows a trend of increasing first and then decreasing with the increase in air flow, which may be due to the fact that the light components and small molecules of the reaction system are quickly taken away by the air purging in the early stage, resulting in the softening point increase. Furthermore, the continuous increase in air flow promotes the

reaction between aromatic free radicals and the oxygen in the air to form aryl free radicals, corresponding to the formation of ether–oxygen bonds, acid anhydride bonds, carbonyl bond bridging products and other polar molecules, changing the fluidity of the asphalt. However, the oxidation transition will lead to the break of some macromolecular chains, and the softening point of the product will decrease [38,39]. When the oxidation temperature is 340 °C, the softening point of the product increases first and then tends to be flat with the increase in air flow. It can be concluded that the high oxidation temperature makes the system react violently, and the free radical polymerization reaction reaches the limit, resulting in coke forming in the product at the later reaction stage. Therefore, the softening point of the product does not increase significantly [40]. As shown in Figure 6, the oxidation temperature, the air flow rate and the softening point of the product are presented as a curved surface relationship graph, and the variation trend of the surface with the independent variable is consistent with the analysis result in Figure 5.

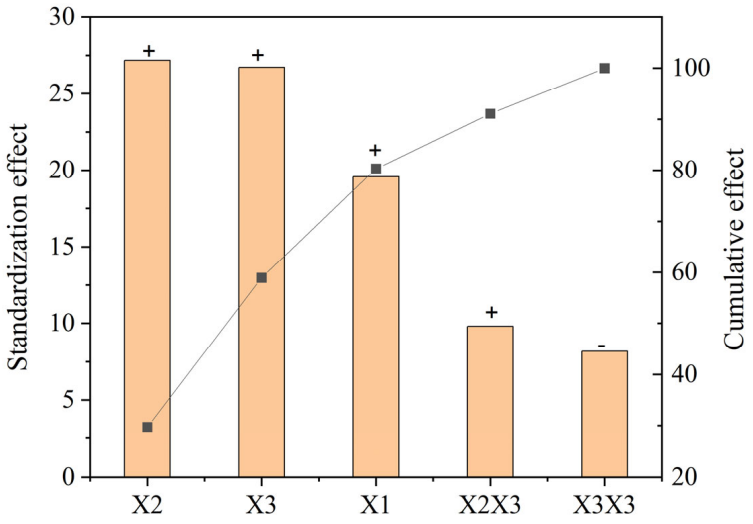


Figure 4. Influence of each factor and its standardization effect on $Y_{softening\ point}$.

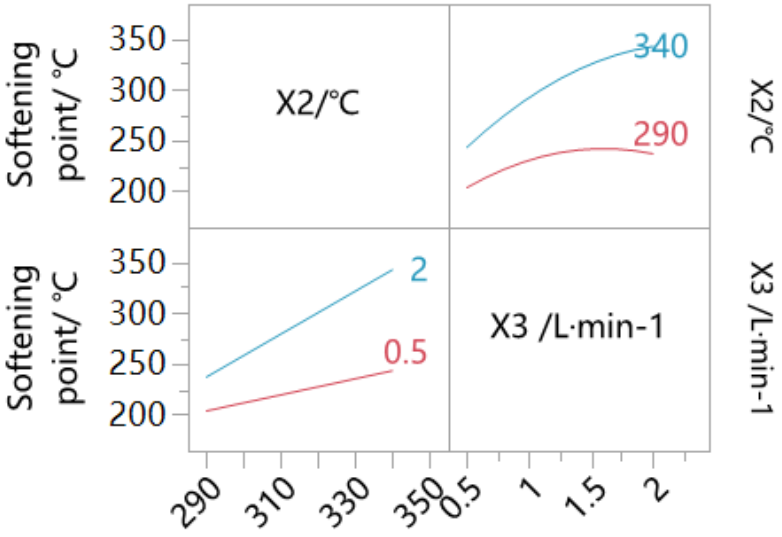


Figure 5. The factor interaction diagram of $Y_{softening\ point}$.

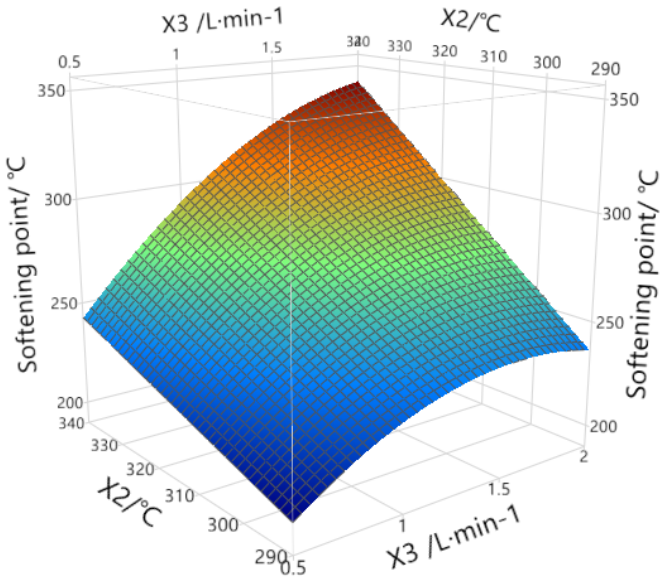


Figure 6. Response surface diagram of $Y_{softening\ point} = f(X_2,\ X_3)$.

3.4. Multiobjective Optimization

Whether the asphalt is used as spinnable asphalt or coated asphalt, the softening point of the product should not be too high. A too high softening point will make the fluidity of the product worse [41,42]. According to the result of the DOE experiment, the softening point of products with a higher coking value is usually higher. Therefore, combined with the downstream application requirements of high softening point asphalt products, it is expected that the softening point of the product is not higher than 310 °C, and the coking value is not higher than 85%. Thus, the upper and lower limits of the two response values and the target values are defined, and the willingness is set by the predictive profiler. After the willingness is maximized, the preparation process parameters satisfying the production of the target product are obtained. Further, a contour profiler is used to provide a range of oxidation process parameters for the production of the target product, as shown in Figures 7 and 8.

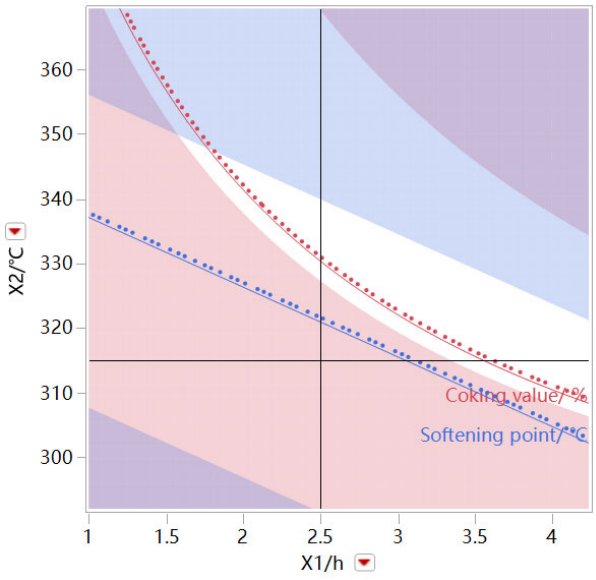


Figure 7. The feasible domain of $Y = f(X_1,\ X_2)$.

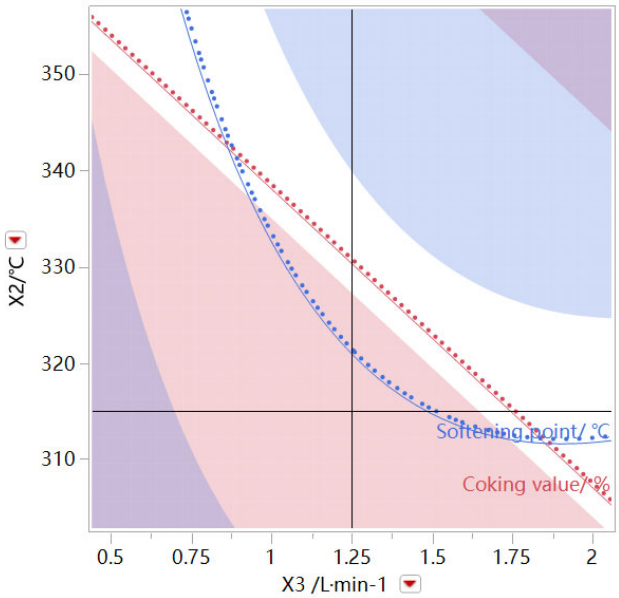


Figure 8. The feasible domain of $Y = f(X_2,\ X_3)$.

As shown in Figure 7, taking the oxidation time and oxidation temperature as variables, the air flow rate is fixed at 1.25 L/min, and the white area is the operational interval of the oxidation time and oxidation temperature, which meets the coking value of the prepared modified asphalt product > 80% and the softening point > 240 °C.

As shown in Figure 8, when the oxidation time is fixed at 2.5 h, the oxidation temperature and air flow are taken as operating variables, and the white area is the operational interval of oxidation temperature and air flow, which meets the coking value of the prepared modified asphalt product > 80% and the softening point > 240 °C. This means that high temperature combined with small air flow rate and low temperature combined with large air flow rate meet the requirements. However, it is recommended that the high temperature and low air flow rate be according to the actual experimental operating conditions, and the large air flow rate will reduce the yield of the product. It can be found that the three factors can be operated in a wide range and that the operation window is wide, under the premise of satisfying the product performance index.

Two groups of process parameters were selected within the operable interval to carry out verification experiments, and the results are shown in Table 7. The coking value and softening point of prepared modified asphalt products were within the predicted interval, indicating that the fitting effect of $Y_{coking\ value}$ and $Y_{softening\ point}$ models is good and reliable.

Table 7. Results of oxidative polymerization test of liquefaction asphalt.

Serial Number	X_1/h	X_2/°C	X_3/L·min^{-1}	Coking Value/%	Softening Point/°C	Coking Value Prediction/%	Softening Point Prediction/°C
1	3.9	330	0.85	81.25	270.0	81.22–84.30	264.6–301.7
2	3.9	330	0.85	82.20	269.8	81.22–84.30	264.6–301.7
3	3.9	330	0.85	81.20	269.4	81.22–84.30	264.6–301.7
4	2.5	315	1.25	80.25	264.1	78.17–80.18	262.9–285.0
5	2.5	315	1.25	79.16	263.7	78.17–80.18	262.9–285.0

3.5. Characterization of Modified Asphalt Products

The asphalts with high softening point were characterized by Fourier infrared test, elemental analysis, C-NMR and MALDI-TOF. As shown in Figures 9–25, the element content, functional group composition, C/O/N/S binding state, aromatic structure and

molecular weight of the product were analyzed, and the relationship between the coking value and softening point of the product and the product composition structure was analyzed, which is helpful to further reveal the mechanism of oxidation.

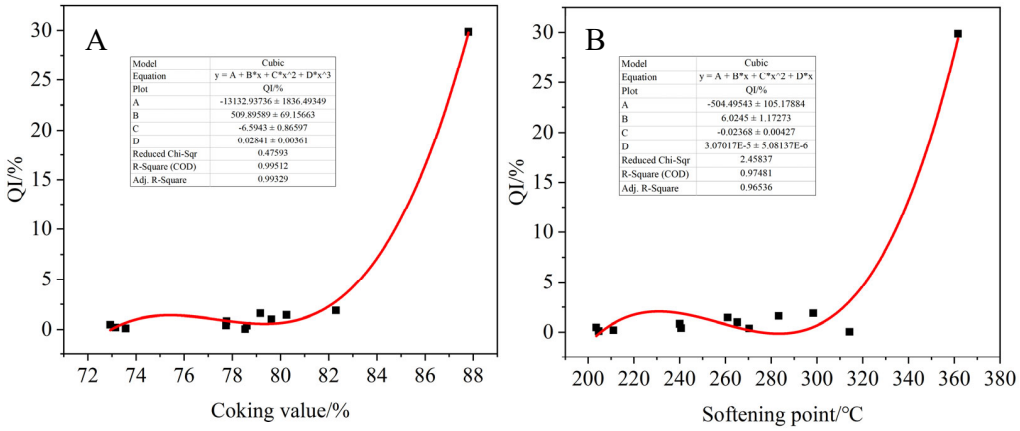


Figure 9. Fitting relationship between QI content of asphalt products and its coking value (**A**) and softening point (**B**).

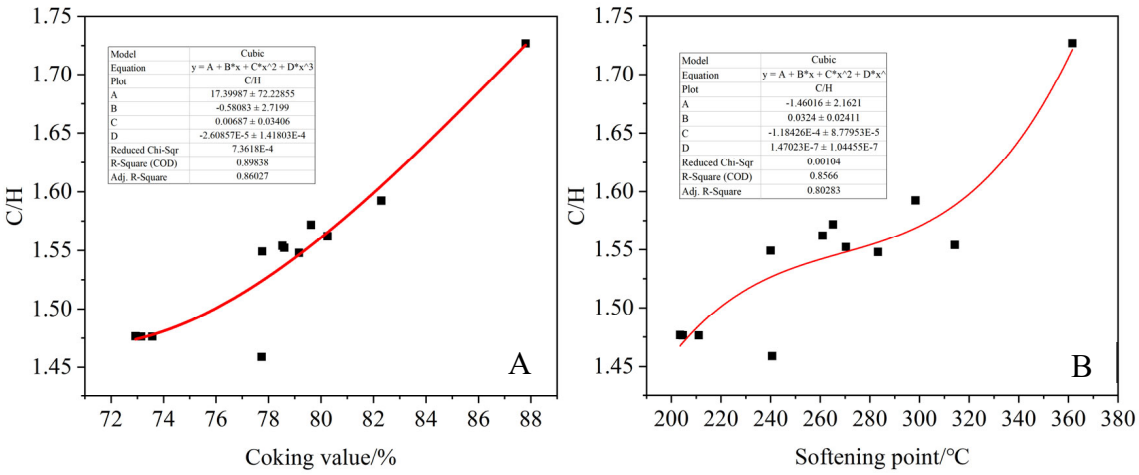


Figure 10. The fitting relationship between C/H ratio of asphalt products and its coking value (**A**) and softening point (**B**).

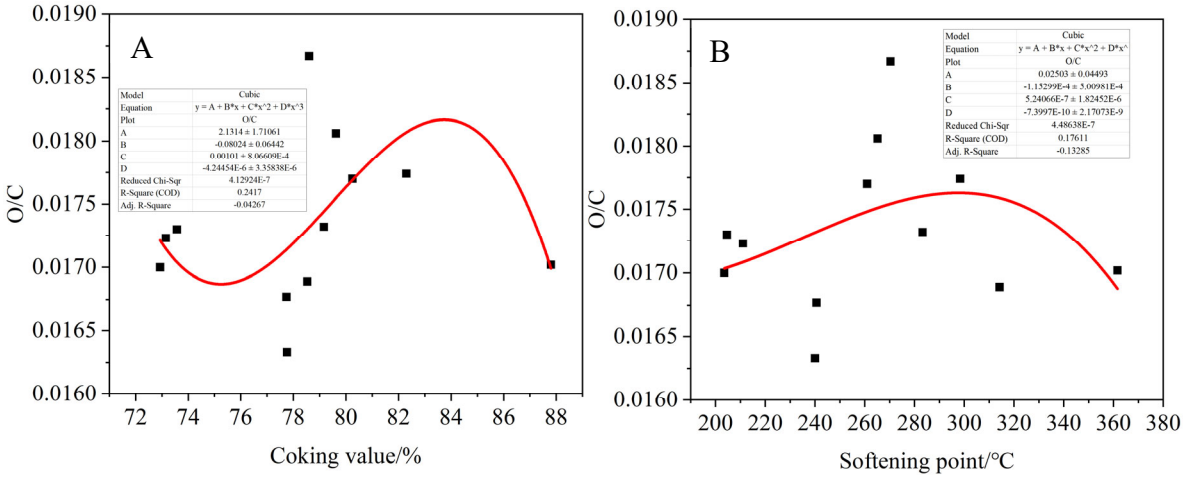


Figure 11. Fitting relationship between O/C of asphalt products and its coking value (**A**) and softening point (**B**).

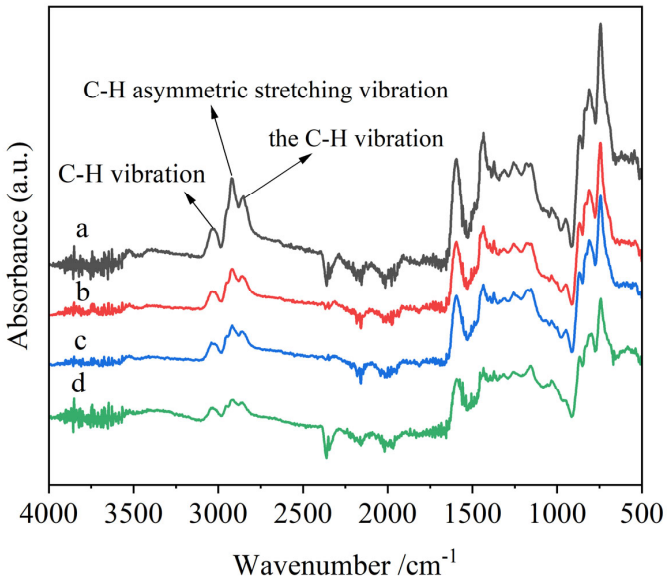


Figure 12. FTIR spectra of asphalt products. a: liquefaction asphalt raw material; b: asphalt products (coking value of 72.9%); c: asphalt products (coking value of 79.2%); d: asphalt products (87.8% coking value).

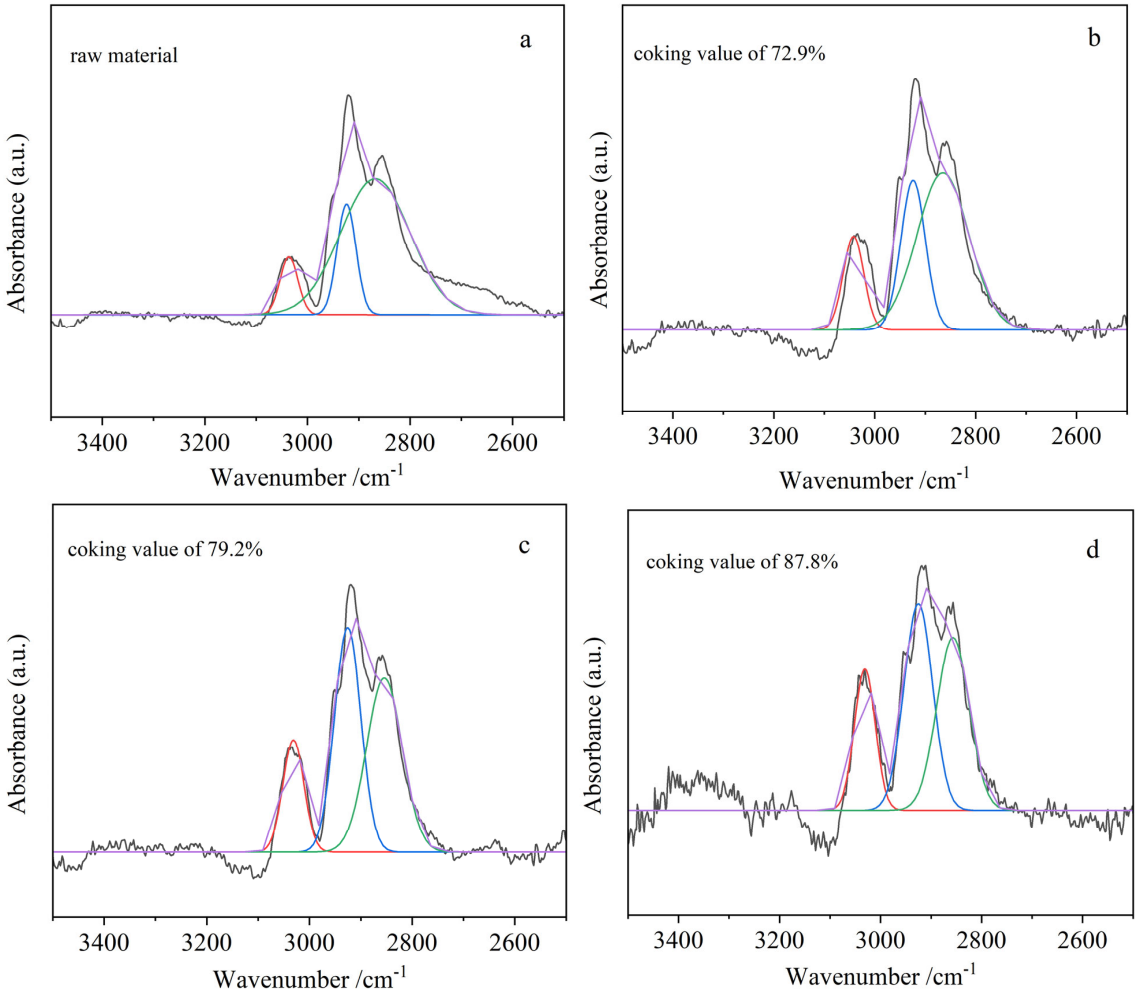


Figure 13. FTIR fitting spectra of asphalt products. (**a**): liquefaction asphalt raw material; (**b**): asphalt products (coking value of 72.9%); (**c**): asphalt products (coking value of 79.2%); (**d**): asphalt products (87.8% coking value).

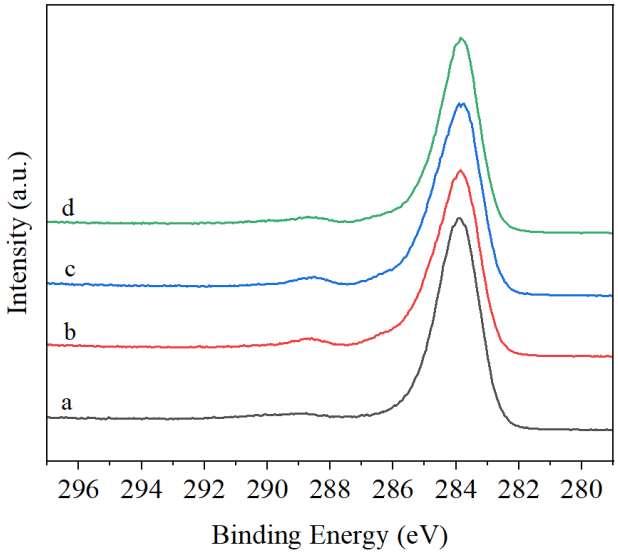


Figure 14. XPS spectra of C1s of asphalt products. a: liquefaction asphalt raw material; b: asphalt products (coking value of 72.9%); c: asphalt products (coking value of 79.2%); d: asphalt products (87.8% coking value).

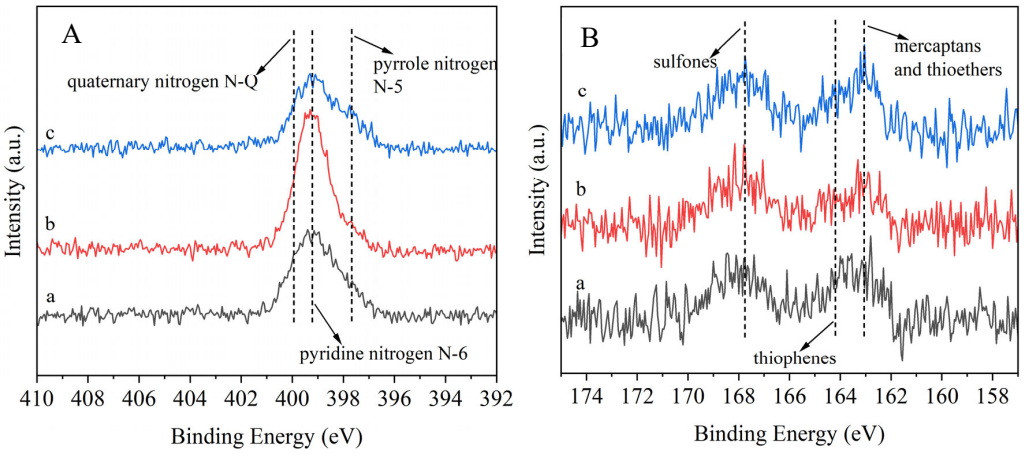


Figure 15. XPS spectra of N1s (**A**) and S2p (**B**) for asphalt products. a: liquefaction asphalt raw material; b: asphalt products (coking value of 72.9%); c: asphalt products (coking value of 79.2%).

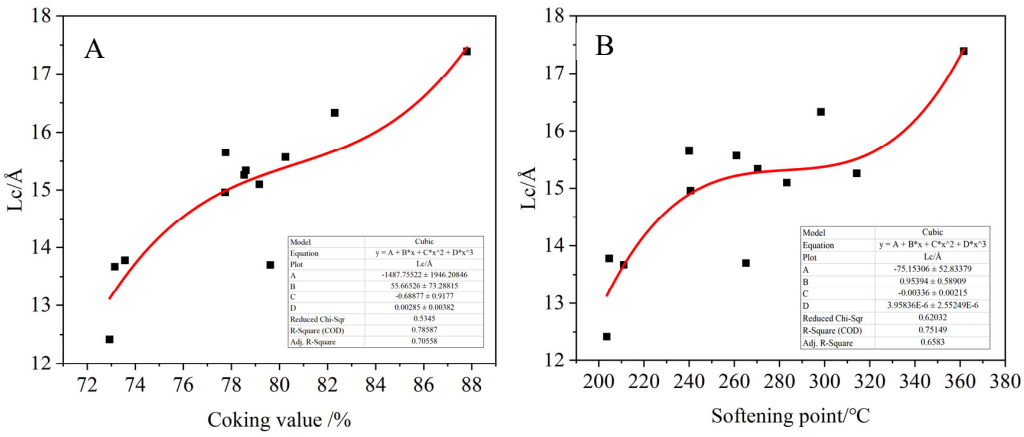


Figure 16. The fitting relationship between the grain size Lc of the asphalt products and its coking value (**A**) and softening point (**B**).

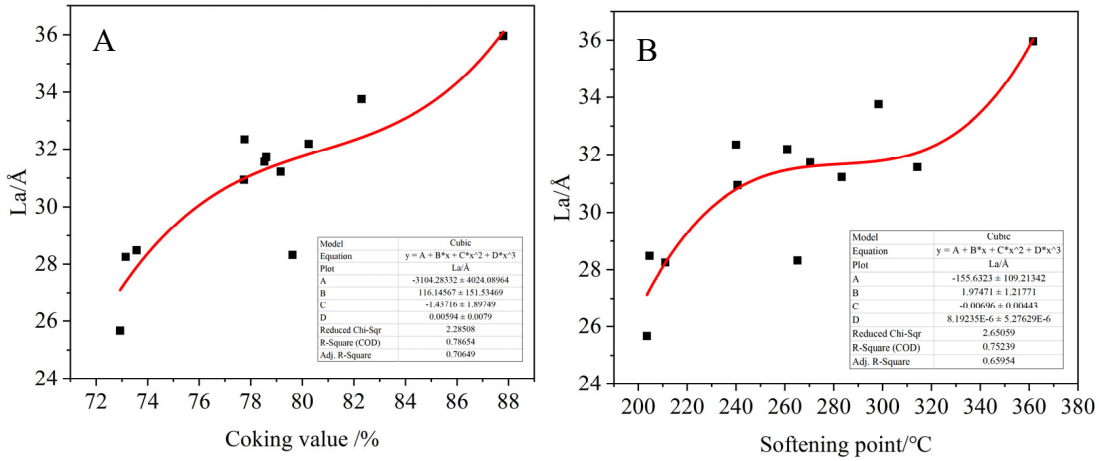


Figure 17. The fitting relationship between grain size La of the asphalt products and its coking value (**A**) and softening point (**B**).

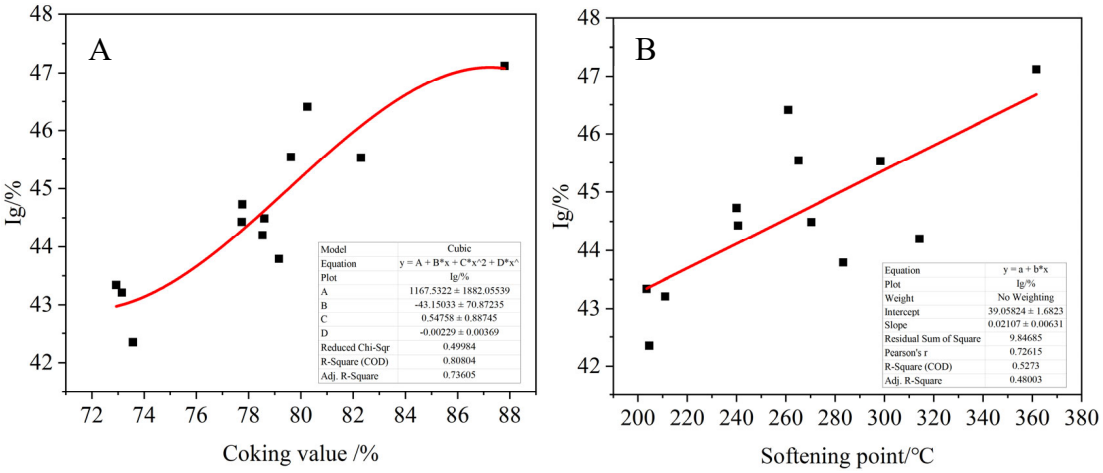


Figure 18. The fitting relationship between the carbon microcrystal content of the asphalt products and its coking value (**A**) and softening point (**B**).

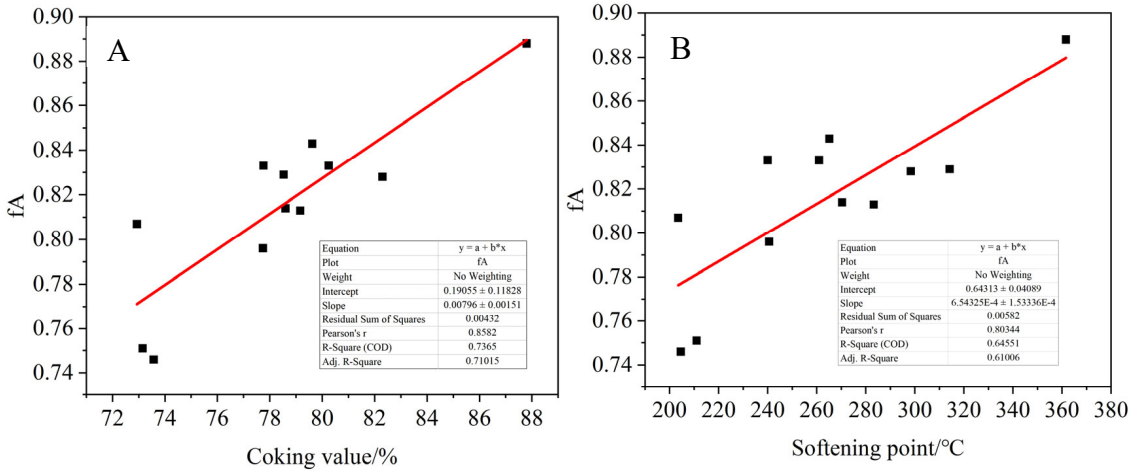


Figure 19. The fitting relationship between the aromaticity of asphalt products and its coking value (**A**) and softening point (**B**).

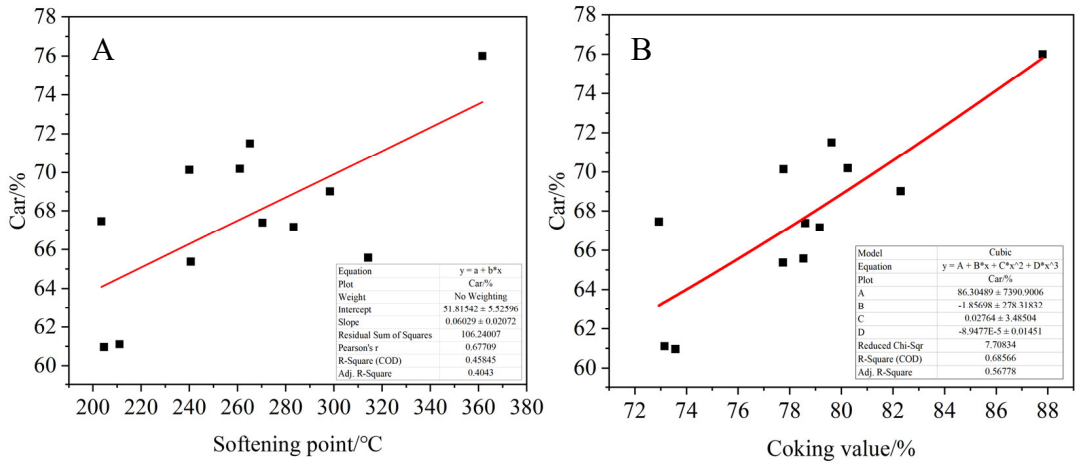


Figure 20. The fitting relationship between the Car proportion of asphalt products and its softening point (**A**) and coking value (**B**).

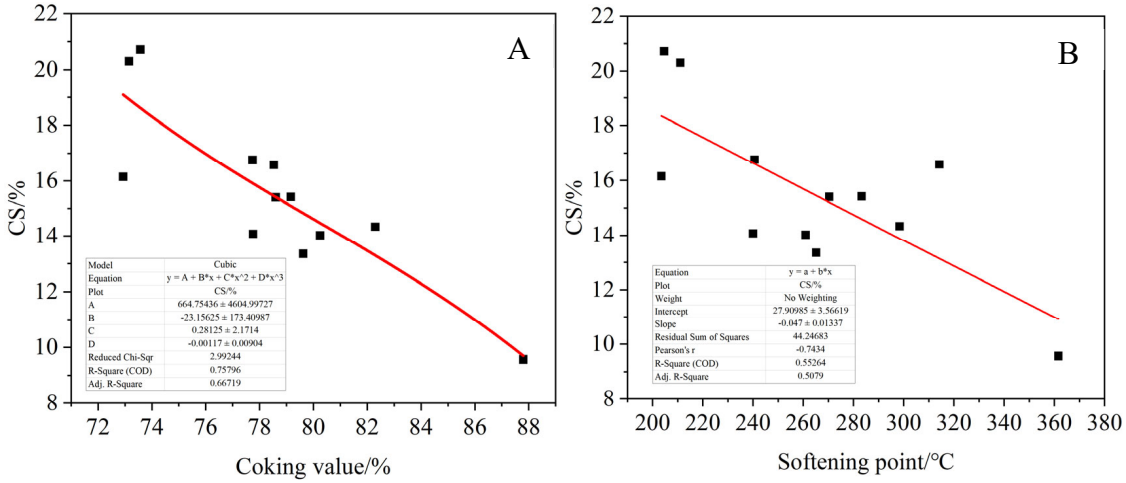


Figure 21. The fitting relationship between Cs proportion of asphalt products and its coking value (**A**) and softening point (**B**).

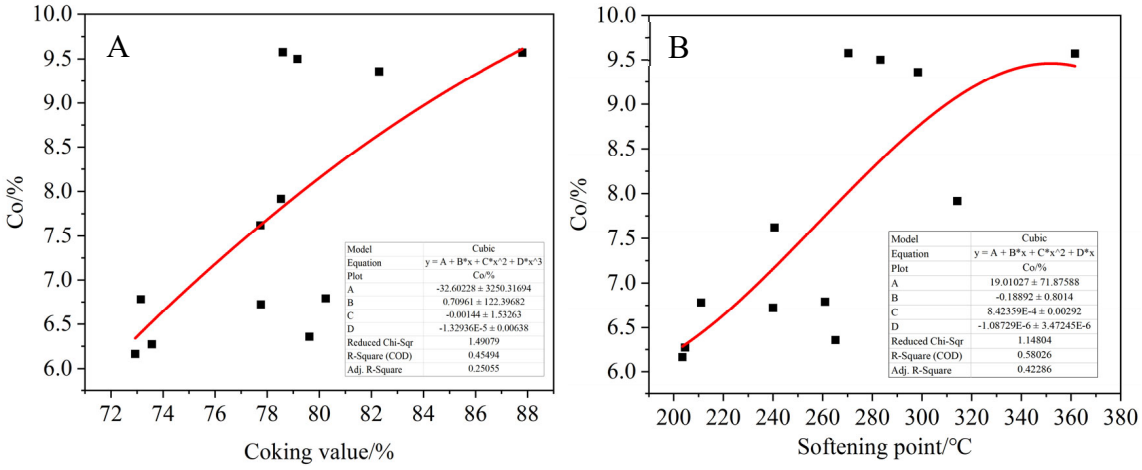


Figure 22. The fitting relationship between the Co ratio of asphalt products and its coking value (**A**) and softening point (**B**).

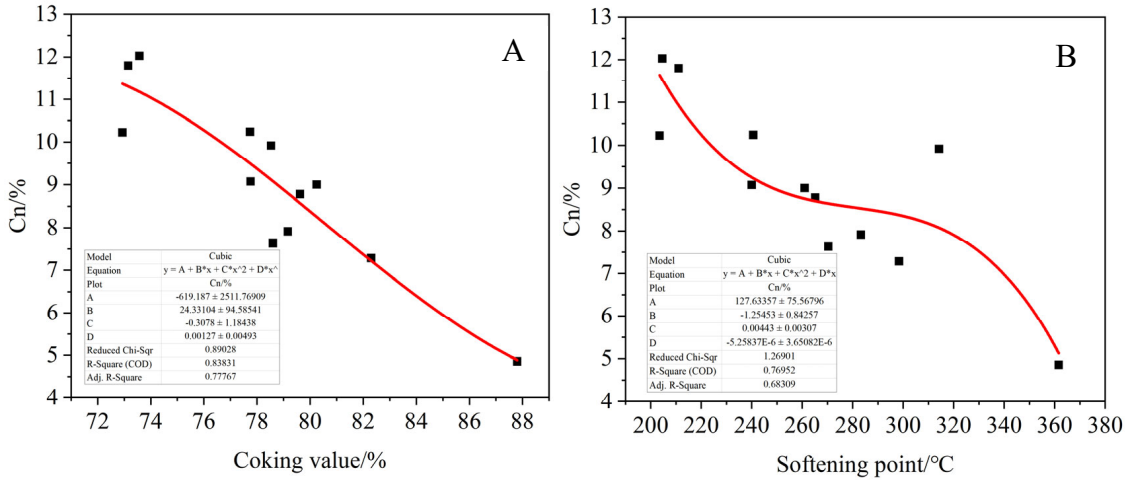


Figure 23. The fitting relationship between Cn ratio of asphalt products and its coking value (**A**) and softening point (**B**).

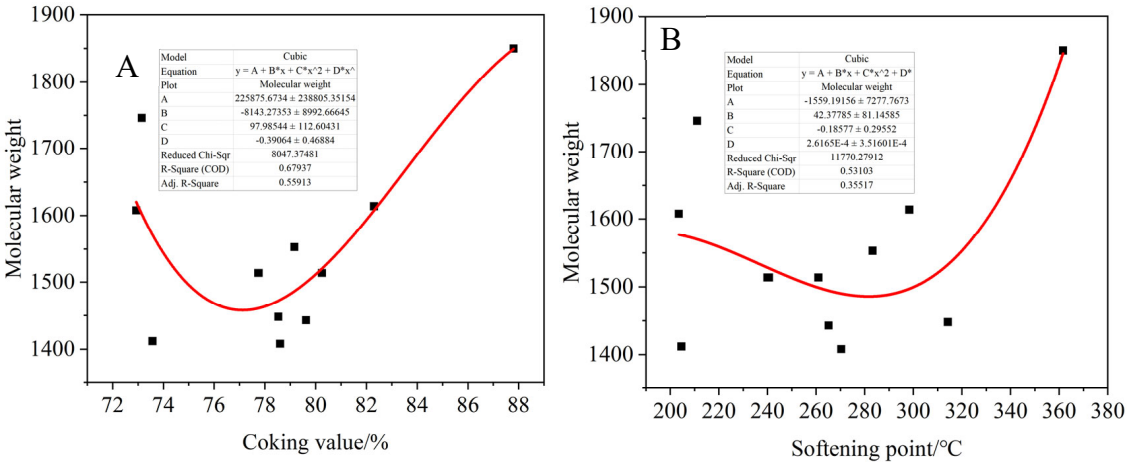


Figure 24. The fitting relationship between the molecular weight of the asphalt products and its coking value (**A**) and softening point (**B**).

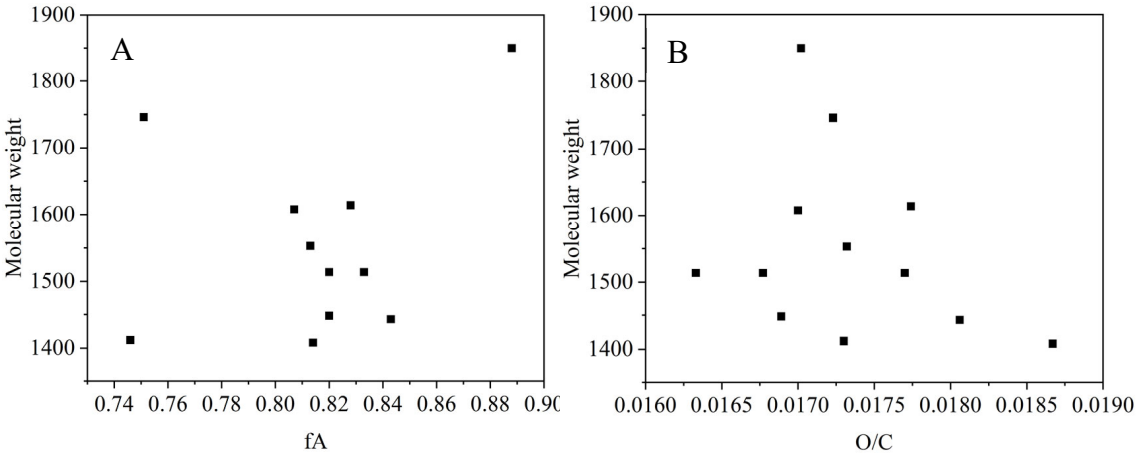


Figure 25. The fitting relationship between the molecular weight of the asphalt products and its aromaticity (**A**) and O/C ratio (**B**).

(1) Composition analysis of asphalt products

As shown in Figure 9, the QI content of modified asphalt obtained after oxidative polymerization is 0.2–30%. When the coking value of the product is bigger than 80% and

the softening point is bigger than 240 °C, the QI content is about 1.5%. However, the QI content is smaller than 1% when the coking value of the product is smaller than 78%. The QI content of the corresponding product increases obviously with the increase in the coking value of the product. When the coking value of the product reaches 87%, the QI content of the corresponding product can reach 30%. With the increase in the oxidation polymerization depth, more light components may escape, and oxygen crosslinked products of macromolecules are formed. As the reaction depth continues to increase, oxygen-containing bridging products may also deoxidize, forming more methylene bridging products, changing the polarity and fluidity of the reaction system making the QI content and softening point of the product significantly increase. On the whole, QI content of products showed an increasing trend with the increase in the coking value and softening point.

(2) Elemental analysis of asphalt products

As shown in Figure 10, the C/H ratio of asphalt products showed an increasing trend with the increase in the coking value and softening point. It can be concluded that the larger the softening point and coking value of the product, the more intense the polymerization reaction, resulting in the formation of more polycyclic aromatic macromolecules. The oxygen content of the product showed a multi-term relationship with the coking value and softening point, and the fitting effect was poor, showing a trend of first increasing and then decreasing, which was consistent with the results of solid C-NMR analysis. It can be indicated that oxidation crosslinking and dealkylation reactions were carried out simultaneously in the reaction process [43]. As shown in Figure 11, with the increase in polymerization reaction degree, the oxidation crosslinking reaction is intense, and the oxygen content in the product increases, resulting in the coking value and softening point of the product increasing. As the degree of reaction continues to increase, the generated oxygen bridging product cracks to produce CO or CO_2, and the oxygen content in the asphalt product decreases, resulting in the O/C ratio and the coking value and softening point of the product showing a trend of first increasing and then decreasing [44].

(3) Infrared spectrum analysis of asphalt products

Figure 12 shows the FTIR spectra of liquefaction asphalt raw materials and corresponding asphalt products with a high softening point. The composition of functional groups in the samples is determined by analyzing the spectra. The C-H vibration peak at 3050 cm^{-1} is the aromatic ring, the C-H vibration peak at 2920 cm^{-1} is the saturated methylene and the C-H asymmetric stretching vibration peak at 2960 cm^{-1} is the saturated methyl [45,46]. Both the asphalt raw materials and the modified asphalt products showed vibration absorption peaks of aromatic ring C=C in the range of 1500–1610 cm^{-1} and 1437 cm^{-1}. The range of 1036–1377 cm^{-1} belongs to the absorption peaks of alkyl side chains and oxygen-containing functional groups, which may be classified as methoxy groups, ether bridge bonds, etc. It can be found that all of these vibration absorption peaks for the asphalt product with a coking value of 87.8% are stronger than that of other products with a lower coking value and raw material, indicating the higher coking value of products with higher polymerization degree and aroma degree. As shown in Figure 13 and Table 8, the aromaticity index (Iar) and branched chain index of the product were determined by peak-splitting fitting of the infrared spectra and calculation of the corresponding peak area. It can be seen from Table 8 that the aromaticity index Iar and branched chain index of the corresponding product increase with the increase in the coking value of the product. It can be inferred that with the increase in the degree of polymerization, the dealkylation reaction occurs strongly, more methylene disappears and a larger dense aromatic molecule is generated. Meanwhile, the product aromaticity increases, and the ratio of saturated

methyl to methylene content increases [47]. All of these results are consistent with the analysis of 13C-NMR and XRD.

Table 8. Structural parameters of coal liquefaction asphalt raw materials and asphalt products.

Samples	A3050	A2960	A2920	Iar	Branched Chain Index
a	8.05	16.47	75.46	0.096	0.218
b	12.92	26.66	59.42	0.179	0.448
c	16.33	40.75	42.90	0.275	0.949
d	20.29	40.90	33.79	0.375	1.210

(4) XPS analysis of asphalt products

Figure 14 shows the XPS spectrum of the prepared modified asphalt products, and Table 9 reveals the results of peak fitting calculation based on XPS spectrum to analyze the binding state of C in the products. It can be seen from the XPS spectra of C1s of the prepared modified asphalt product that C=C content in the products increases with the increase in the coking value. The results showed that more aromatic compounds were formed with the increase in oxidation polymerization depth, consistent with the analysis of NMR and XRD. At the same time, the proportion of carbon and oxygen functional groups in the product increases first and then decreases with the increase in the coking value. Compared with the liquefaction asphalt raw material, when the coking value of the product is 72.9% and 79.2%, respectively, the content of carbon and oxygen functional groups in the product increases, indicating that an oxidation crosslinking reaction occurs. In addition, the content of carbon and oxygen functional groups in the product decreases with the coking value of the product increased to 87.8%, which should be due to the ether bond, anhydride bond and carbonyl bond compounds generated by oxidative crosslinking reaction undergoing cracking and decarboxylation reactions to produce CO and CO_2 and other substances.

Table 9. Analysis of C1s XPS of asphalt raw materials and asphalt products.

Samples	-C=C-/%	-C-C-/%	-C-O-/%
	283.1 ± 0.3 eV	**283.9 ± 0.3 eV**	**287.5 ± 1.0 eV**
a	57.91	32.05	10.04
b	60.90	27.27	11.82
c	62.79	25.34	12.56
d	67.66	21.31	11.03

It can be seen from Figure 15 that both raw material and modified asphalt products contain nitrogen and sulfur elements, and the analytical results are consistent with those of elemental analysis. Furthermore, the presence of sulfur and nitrogen can be determined by XPS spectrogram analysis of N1s and S2p. Combined with the XPS map of N1s, chemical state and location information of nitrogen in raw material and products is as follows: pyrrole nitrogen N-5 (399.0 ± 0.5 eV), pyridine nitrogen N-6 (398.0 ± 0.5 eV) and quaternary nitrogen N-Q (400.0 ± 0.5 eV), which mainly exists in the form of pyrrole nitrogen N-5 [48–50]. Given that the coal liquefaction asphalt has the characteristics of low sulfur, it can be further certified by elemental analysis. According to the XPS of S2p, the chemical state and location information of sulfur in raw materials and products is as follows: mercaptans and thioethers (163.0 ± 0.5 eV), thiophenes (164.2 ± 0.5 eV) and sulfones (168.5 ± 0.5 eV), which mainly exist in the form of organic sulfur and sulfones [51].

(5) XRD analysis of asphalt products

The crystal structure parameters, the grain size La and Lc and the carbon microcrystal content Ig were calculated by the XRD pattern of the modified asphalt products. The fitting relationship between the grain size and carbon microcrystal content of the products and the coking value and softening point of the products are shown in Figures 16–18. It can be found that the carbon microcrystal content of the products is positively correlated with the coking value of the product, and there is a polynomial relationship with the softening point, but the general trend is that the degree of graphitization of the product increases with the increase in the softening point. The grain size La and Lc are positively correlated with the softening point and coking value of the product, indicating that products with a higher coking value correspond to higher graphitization degree and larger grain size. Meanwhile, the analysis results are consistent with the results of FTIR and XPS analysis.

(6) NMR analysis of asphalt products

The proportion of saturated carbon, normal alkane carbon, aromatic carbon and carbon–oxygen functional groups in the product were calculated according to 13C-NMR spectra of the asphalt product. As shown in Figures 19–23, the relationships between the proportion of each functional group and the coking value and softening point of the product were fitted. Among them, 5–60 ppm represents saturated carbon CS, 25–50 ppm represents normal alkane carbon Cn, 110–160 ppm represents aromatic carbon Car and 188–230 ppm represents carbonyl carbon Co, which is associated with oxygen. It can be seen that the ratio of aromatic carbon Car of the product increases with the increase in the softening point and coking value of the product. On the contrary, the ratio of saturated carbon Cs to normal alkane carbon decreased, and the carbonyl carbon content of the product also showed an increasing trend with the increase in the softening point and coking value, but the fitting effect was poor. This indicates that the larger the product coking value, the more layered thick cyclic aromatic hydrocarbons are generated, resulting in the asphalt product having a higher aromatic degree. In addition, when more alkyl side chains are broken, the corresponding product has less saturated carbon and normal alkane carbon. At the same time, the oxidation crosslinking reaction is intensified in the transitional oxidation state, and more carbonyl compounds are generated.

(7) Molecular weight analysis of asphalt products

As shown in Figures 24 and 25, the fitting relationship between the molecular weight and the coking value, softening point, aromaticity and O/C of the product were obtained. The molecular weight of the product decreases first and then increases with the increase in the coking value and softening point. The increase in the coking value means that the polymerization degree increases. At the beginning, the alkyl side chain breaks and some small molecules are purged out, resulting in a slight decrease in the molecular weight of the product. With the progress of oxidation polymerization, the condensation polymerization and crosslinking reaction are intensified, while more dense aromatic hydrocarbons are formed, and the molecular weight of the products in the reaction system increases. At the same time, the molecular weight of the asphalt products did not change significantly with the aromatic degree and O/C ratio.

3.6. Verification of Spinning Performance

Preliminary spinning verification of the target product (coking value of 80.25%) showed that continuous spinning could be carried out at a high spinning speed (600–800 r/min), indicating that the prepared modified asphalt with high softening point had good spinnability. Therefore, the liquefaction asphalt carbon fiber (LACF) was obtained by spinning, pre-oxidation and carbonization of the target product. Meanwhile,

the commercially general grade asphalt carbon fiber (MCP) was purchased from a certain enterprise in Shandong, China, and was prepared by coal tar asphalt. The morphology and structure of the LACF and MCF were analyzed by SEM, and the diameter was calculated, as shown in Figure 26.

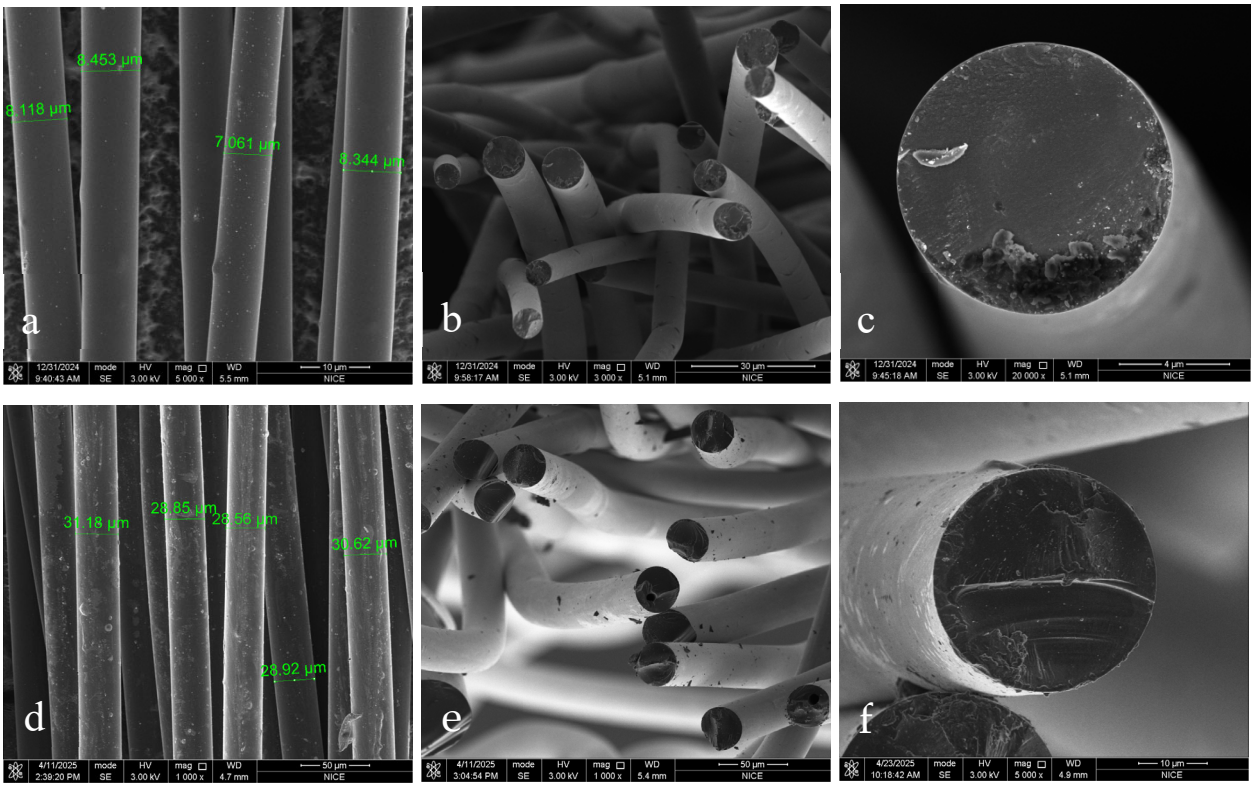


Figure 26. Morphology and structure analysis of carbonized fiber ((**a**–**c**): LACF; (**d**–**f**): MCF).

As shown in Figure 26a–c, there were no splitting or cavity defects inside the carbon fiber (LACF), the surface was relatively smooth and the diameter of the fiber was 8–10 µm. However, the fracture section of carbon fiber from market (MCF) has air holes, and the surface is uneven, as shown in Figure 26d–f, which may be due to the composition distribution of spinnable asphalt being relatively wide. As shown in Table 10, the mechanical properties of the carbon fibers were evaluated by fiber strength meter. For the LACF, the tensile strength, elastic modulus and elongation at break were 775 MPa, 68.6 GPa and 1.13%, respectively, which is better than the mechanical properties of MCF. This may be due to the fact that the liquefaction asphalt has a higher hydrogen content compared to coal tar asphalt, so the fluidity of the corresponding spinnable asphalt is better, which can be further proved by the diameter of the carbon fibers. Therefore, the liquefaction asphalt carbon fiber has value for further study.

Table 10. The mechanical properties of the carbon fibers.

Samples	Tensile Strength/MPa	Elastic Modulus/GPa	Elongation at Break/%	Diameter/µm
LACF	775	68.6	1.13	8
MCF	474	37.7	1.20	29

4. Conclusions

In this work, the modified asphalt with high softening point was prepared by air oxidation polymerization using the high grade coal liquefaction asphalt. The prediction

models of the softening point and coking value of the product were obtained by the response surface analysis method. The quality of the prediction model is reliable, and the prediction effects are good. It can be found that the oxidation temperature, oxidation time and air flow rate are positively correlated with the coking value and softening point of the product. Meanwhile, the oxidation process parameters which meet the requirements of target products (coking value > 80%, softening point > 240 °C) are determined. According to the results of the product composition and structure analysis, the aromaticity I_{ar}, the branched chain index and the C/H ratio of products increase with the increase in the coking value. In the process of the oxidation reaction, the alkyl side chain of the liquefaction asphalt breaks to form aryl free radicals, and the aryl free radicals interact with oxygen in the air to form alkoxy radicals, which leads to the free radical polymerization reaction. Furthermore, aromatic molecules in the asphalt generate polycyclic aromatic hydrocarbons with larger molecular weight through oxygen bridge bonds. In addition, the spinnability of the target product is good, and the performance of the preliminarily prepared carbon fiber is better than that of the general grade fiber on the market, which has further research value.

Author Contributions: Resources, Writing—review & editing, Y.L.; Writing—original draft, C.J.; Resources, M.G. All authors have read and agreed to the published version of the manuscript.

Funding: This work was supported by a grant from the National Energy Investment Group Technology Innovation Project of China (No. S930024041).

Data Availability Statement: The original contributions presented in this study are included in the article. Further inquiries can be directed to the corresponding author.

Acknowledgments: This work was supported by the Ordos Coal to Liquid Branch and National Institute of Clean and Low Carbon Energy. We thank them for their help and support, as well as the funding received from the Ordos Coal to Liquid Branch of China Shenhua Coal to Liquid and Chemical Co., Ltd.

Conflicts of Interest: Authors Yong Liu and Miao Gao were employed by the company Ordos Coal to Liquid Branch of China Shenhua Coal to Liquid and Chemical Co., Ltd. Author Chenguang Jiang was employed by the company National Institute of Clean and Low Carbon Energy. The company had no role in the design of the study; in the collection, analyses, or interpretation of data; in the writing of the manuscript, or in the decision to publish the results.

References

1. Li, J.; Yang, J.; Liu, Z. Hydrogenation of heavy liquids from a direct coal liquefaction residue for improved oil yield. *Fuel Process. Technol.* **2009**, *90*, 490–495. [CrossRef]
2. Dutta Majumdar, R.; Bake, K.D.; Ratna, Y.; Pomerantz, A.E.; Mullins, O.C.; Gerken, M.; Hazendonk, P. Single-core PAHs in petroleum and coal-derived asphaltenes: Size and distribution from solid-state NMR spectroscopy and optical absorption measurements. *Energy Fuels* **2016**, *30*, 6892–6906. [CrossRef]
3. Cheng, J.; Zhu, Y.; Gao, L.; Zhao, X.-f. Structural characterizations of coal tar pitch as needlecoke raw material by H-NMR and FT-IR. *Carbon Tech.* **2019**, *38*, 24–27.
4. Mao, X.; Li, J.; Zhong, J.; Shi, Q.; Yan, B.; Liu, M. Composition and structure molecular characterizations of medium and low temperature coal tar. *J. China Coal Soc.* **2019**, *44*, 957–963.
5. Lin, H.; Li, K.; Zhang, X.; Wang, H.; Cheng, S. Analysis and structural model of coal lique faction asphaltene. *J. Fuel Chem. Technol.* **2014**, *42*, 779–784.
6. Zhu, Y.; Huang, J.; Dan, Y.; Wang, L.; Li, W.; Li, D. Analysis and Charactrization of Medium/Low Temperature Coal Tar Asphaltene. *Acta Pet. Sin. (Pet. Process Sect.)* **2016**, *32*, 334–342.
7. Burgess, W.A.; Thies, M.C. Molecular structures for the oligomeric constituents of petroleum pitch. *Carbon* **2011**, *49*, 636–651. [CrossRef]
8. Lin, X.; Sheng, Z.; He, J.; Wang, Y. Preparation of isotropic spinnable pitch with high-spinnability by co-carbonization of coal tar pitch and bio-asphalt. *Fuel* **2021**, *295*, 120627. [CrossRef]

9. Kim, B.-H.; Kim, J.-H.; Kim, J.-G.; Bae, M.-J.; Im, J.S.; Lee, C.W.; Kim, S. Electrochemical and structural properties of lithium battery anode materials by using a molecular weight controlled pitch derived from petroleum residue. *J. Ind. Eng. Chem.* **2016**, *41*, 1–9. [CrossRef]
10. Yamaguchi, C.; Mondori, J.; Matsumoto, A.; Honma, H.; Kumagai, H.; Sanada, Y. Air-blowing reactions of pitch: I. Oxidation of aromatic hydrocarbons. *Carbon* **1995**, *33*, 193–201. [CrossRef]
11. Huang, L.; Su, G.; Luo, W. Study on the interfacial mechanical properties of graphene oxide modified asphalt based on molecular dynamics simulation. *J. Wuhan Univ. Sci. Technol.* **2025**, *48*, 1–10.
12. Wang, W.; Liu, G.; Shen, J.; Chang, H.; Li, R.; Du, J.; Yang, Z.; Xu, Q. Reducing polycyclic aromatic hydrocarbons content in coal tar pitch by potassium permanganate oxidation and solvent extraction. *J. Environ. Chem. Eng.* **2015**, *3*, 1513–1521. [CrossRef]
13. Pérez, M.; Granda, M.; Santamaría, R.; Morgan, T.; Menéndez, R. A thermoanalytical study of the co-pyrolysis of coal-tar pitch and petroleum pitch. *Fuel* **2004**, *83*, 1257–1265. [CrossRef]
14. Ge, C.; Sun, Z.; Yang, H.; Long, D.; Qiao, W.; Ling, L. Preparation and characterization of high softening point and homogeneous isotropic pitches produced from distilled ethylene tar by novel bromination method. *New Carbon Mater.* **2018**, *33*, 71–81. [CrossRef]
15. Farokhi, S.; Roushani, M. Flower-like core-shell nanostructures based on natural asphalt coated with Ni-LDH nanosheets as an electrochemical platform for prostate cancer biomarker sensing. *Microchim. Acta* **2023**, *190*, 198. [CrossRef] [PubMed]
16. Li, P.P.; Xiong, J.M.; Ge, M.L.; Sun, J.C.; Zhang, W.; Song, Y.Y. Preparation of pitch-based general purpose carbon fibers from catalytic slurry oil. *Fuel Process. Technol.* **2015**, *140*, 231–235. [CrossRef]
17. Guo, T.-r.; Chen, R.-q.; Gao, W.; Wang, Y.-l.; Zhan, L. The oxidation reaction mechanism and its kinetics for a carbonaceous precursor prepared from ethylene tar for use as a cathode material for lithium-ion batteries. *New Carbon Mater.* **2024**, *39*, 354–366. [CrossRef]
18. Fernández, J.J.; Figueiras, A.; Granda, M.; Bermejo, J.; Menéndez, R. Modification of coal-tar pitch by air-blowing-I. Variation of pitch composition and properties. *Carbon* **1995**, *33*, 295–307. [CrossRef]
19. Zhou, Y.; Xiao, N.; Qiu, J.; Sun, Y.; Sun, T.; Zhao, Z.; Zhang, Y.; Tsubaki, N. Preparation of carbon microfibers from coal liquefaction residue. *Fuel* **2008**, *87*, 3474–3476. [CrossRef]
20. *GB/T 2294-2019*; Determination of Softening Point in Solid Products of Coal Carbonization. Standards Press of China: Beijing, China, 2019.
21. *ISO 5940-2:2007*; Carbonaceous Materials Used in the Production of Aluminum—Pitch for Electrodes—Part 2: Determination of the Softening Point (Mettler Softening Point Method), Respectively. ISO: Geneva, Switzerland, 2007.
22. *GB/T 2293-2019*; The Method of Quinoline-Insoluble for Pitch Products of Coal Carbonization. Standards Press of China: Beijing, China, 2019.
23. *SH/T 0656-2017*; Determination of Carbon, Hydrogen and Nitrogen in Petroleum Products and Lubricants Elemental Analyzer Method. National Energy Administration: Beijing, China, 2017.
24. *SH/T 0704-2010*; Standard Test Method for Nitrogen in Petroleum and Petroleum Products by Boat-Inlet Chemiluminescence. National Energy Administration: Beijing, China, 2010.
25. *GB/T 17040-2008*; Standard Test Method for Sulfur in Petrolem and Petroleum Products by Energy Dispersive X-ray Fluorescence Spectrometry. Standards Press of China: Beijing, China, 2008.
26. *SH/T 0986-2019*; Standard Test Method for Determination of Total Oxygen in Gasoline, Diesel and Methanol Fuels by Reductive Pyrolysis. National Energy Administration: Beijing, China, 2019.
27. Manoj, B.; Kunjomana, A.G. Study of stacking structure of amorphous carbon by X-Ray diffraction technique. *Int. J. Electrochem. Sci.* **2012**, *7*, 3127–3134. [CrossRef]
28. Sonibare, O.O.; Haeger, T.; Foley, S.F. Structural characterization of nigerian coals by X-ray diffraction, Raman and FTIR spectroscopy. *Energy* **2010**, *35*, 5347–5353. [CrossRef]
29. Kim, J.D.; Roh, J.S.; Kim, M.S. Effect of carbonization temperature on crystalline structure and properties of isotropic pitch-based carbon fiber. *Carbon Lett.* **2017**, *21*, 51–60. [CrossRef]
30. Michael, G.; Al-Siri, M.; Khan, Z.H.; Ali, F.A. Differences in Average Chemical Structures of Asphaltene Fractions Separated from Feed and Product Oils of a Mild Thermal Processing Reaction. *Energy Fuels* **2005**, *19*, 1598–1605. [CrossRef]
31. Trejo, F.; Ancheyta, J.; Centeno, G.; Marroquín, G. Effect of hydrotreating conditions on Maya asphaltenes composition and structural parameters. *Catal. Today* **2005**, *109*, 178–184. [CrossRef]
32. Eslami, A.; Asadi, A.; Meserghani, M.; Bahrami, H. Optimization of sonochemical degradation of amoxicillin by sulfate radicals in aqueous solution using response surface methodology (RSM). *J. Mol. Liq.* **2016**, *222*, 739–744. [CrossRef]
33. Wei, W.; Jiang, C. Optimization of the Preparation Process of Refined Asphalt Based on the Response Surface and Preparation of Needle coke. *ACS Omega* **2024**, *9*, 13239–13251. [PubMed]
34. Noordin, M.Y.; Venkatesh, V.C.; Sharif, S.; Elting, S.; Abdullah, A. Application of response surface methodology in describing the performance of coated carbide tools when turning AISI 1045 steel. *J. Mater. Process. Technol.* **2004**, *145*, 46–58. [CrossRef]

35. Ghafari, S.; Aziz, H.A.; Isa, M.H.; Zinatizadeh, A.A. Application of response surface methodology (RSM) to optimize coagulation-flocculation treatment of leachate using poly-aluminum chloride (PAC) and alum. *J. Hazard. Mater.* **2009**, *163*, 650–656. [CrossRef]
36. Chen, X.; Jiang, C.; He, X.; Zhang, C.; Lin, X.; Lan, X. Optimization of the Carbonization Process for the Preparation of High-Grade Needle Coke Based on the Response Surface Method and Microstructure Analysis. *ACS Omega* **2024**, *9*, 46349–46361. [CrossRef]
37. Barr, J.B.; Lewis, I.C. Chemical changes during the mild air oxidation of pitch. *Carbon* **1978**, *16*, 439–444. [CrossRef]
38. Metzinger, T.; Hüttinger, K.J. Investigations on the crosslinking of binder pitch matrix of carbon bodies with molecular oxygen-part I. Chemistry of reactions between pitch and oxygen. *Carbon* **1997**, *35*, 885–892. [CrossRef]
39. Fernández, A.L.; Granda, M.; Bermejo, J.; Menéndez, R. Air-blowing of anthracene oil for carbon precursors. *Carbon* **2000**, *38*, 1315–1322. [CrossRef]
40. Lewis, I.C.; Singer, L.S. Electron spin resonance study of the reaction of aromatic hydrocarbons with oxygen. *J. Phys. Chem.* **1981**, *85*, 354–360. [CrossRef]
41. Zeng, S.M.; Maeda, T.; Tokumitsu, K.; Mondori, J. Preparation of isotropic pitch precursors for general purpose carbon fibers (GPCF) by air blowing-III. Air blowing of isotropic naphthalene and hydrogenated coal tar pitches with addition of 1, 8-dinitronaphthalene. *Carbon* **1993**, *31*, 421–426. [CrossRef]
42. Alcañiz-Monge, J.; Cazorla-Amorós, D.; Linares-Solano, A.; Oya, A.; Sakamoto, A.; Hosm, K. Preparation of general purpose carbon fibers from coal tar pitches with low softening point. *Carbon Int. J. Spons. By Am. Carbon Soc.* **1997**, *35*, 1079–1087. [CrossRef]
43. Mochida, I.; Inaba, T.; Korai, Y.; Fujitsu, H.; Takeshita, K. Carbonization properties of carbonaceous substances oxidized by air blowing-I: Carbonization behaviors and chemical structure of residual oils oxidized by air blowing. *Carbon* **1983**, *21*, 543–552. [CrossRef]
44. Matsumoto, T.; Mochida, I. A structural study on oxidative stabilization of mesophase pitch fibers derived from coal tar. *Carbon* **1992**, *30*, 1041–1046. [CrossRef]
45. Zhu, Y.; Zhao, X.; Gao, L.; Jun, L.; Cheng, J.; Lai, S. Properties and micro-morphology of primary quinoline insoluble and mesocarbon microbeads. *J. Mater. Sci.* **2016**, *51*, 8098–8107. [CrossRef]
46. Zhu, Y.; Zhao, X.; Gao, L.; Jun, L.; Cheng, J.; Lai, S. Study on the Pyrolysis Characteristic and the Microstructure of the Pyrolysis Products of beta Resins from Different Coal Tar Pitch. *J. Chem. Soc. Pak.* **2018**, *40*, 343–353.
47. Yang, C.Q.; Simms, J.R. Infrared spectroscopy studies of the petroleum pitch carbon fiber-I: The raw materials, the stabilization, and carbonization processes. *Carbon* **1993**, *31*, 451–459. [CrossRef]
48. Liu, S.; Wei, M.; Qiao, Y.; Yang, Z.; Gui, B.; Yu, Y.; Xu, M. Release of organic sulfur as sulfur-containing gases during low temperature pyrolysis of sewage sludge. *Proc. Combust. Inst.* **2015**, *35*, 2767–2775. [CrossRef]
49. Kelemen, S.R.; Afeworki, M.; Gorbaty, M.L.; Sansone, M.; Kwiatek, P.J.; Walters, C.C.; Freund, H.; Siskin, M.; Bence, A.E.; Curry, D.J.; et al. Direct characterization of Kerogen by X-ray and solid-state 13C nuclear magnetic resonance methods. *Energy Fuels* **2007**, *21*, 1548–1561. [CrossRef]
50. Kozłowski, M. XPS study of reductively and non-reductively modified coals. *Fuel* **2004**, *83*, 259–265. [CrossRef]
51. Ding, D.; Liu, G.; Fu, B.; Yuan, Z.; Chen, B. Influence of magmatic intrusions on organic nitrogen in coal: A case study from the Zhuji mine, the Huainan coalfield, China. *Fuel* **2018**, *219*, 88–93. [CrossRef]

Disclaimer/Publisher's Note: The statements, opinions and data contained in all publications are solely those of the individual author(s) and contributor(s) and not of MDPI and/or the editor(s). MDPI and/or the editor(s) disclaim responsibility for any injury to people or property resulting from any ideas, methods, instructions or products referred to in the content.